SSRG International Journal of Electronics and Communication Engineering
ISSN: 2348-8549/ https://doi.org/10.14445/23488549/IJECE-V13I5P109

Volume 13 Issue 5, 88-96, May 2026

Original Article

Handcrafted-Guided, Token Fusion with Learnable Attention Priors for Robust Lung and Colon Histopathology Subtype Recognition

Mullakuri Anusha[1], D. Srinivasulu Reddy[2]

[1]*Department of Electronics and Communication Engineering, Jawaharlal Nehru Technological University, Anantapur, Anantapuramu, India.*
[2]*Department of ECE, Sri Venkateswara College of Engineering, Tirupati, Affiliated to Jawaharlal Nehru Technological University, Anantapur, Anantapuramu, India.*

[2]*Corresponding Author : mullakurianusha@gmail.com*

Received: 08 February 2026 Revised: 10 March 2026 Accepted: 10 April 2026 Published: 27 May 2026

Abstract *- Precise multi-class classification of lung and colon histopathology is of great clinical value but still poses a challenge because of the variability of stains and the subtle overlap of morphologies among different types of tissue. In this paper, a lightweight hybrid approach is proposed for the five-class classification of LC25000 patches (benign colon, benign lung, colon adenocarcinoma, lung adenocarcinoma, and lung squamous cell carcinoma). The proposed approach learns deep spatial morphology features from a convolutional encoder and represents compact handcrafted stain-prior features by L1-normalized RGB histograms. The novelty of this work is the employment of pre-pooling token fusion by means of directional handcrafted-to-morphology cross-attention, which is further reinforced by a learnable bias to improve the robustness of color-region affinity learning against appearance variation. The fused features are then enhanced by residual feed-forward blocks and classified by a compact head. The experimental results show that the proposed approach can bring consistent improvements in class-wise discrimination and agreement above chance level over attention and late fusion baselines, with accuracy, macro-F1, macro-AUC, and Cohen's κ values of 0.9947, 0.9947, 0.9999, and 0.9933, respectively.*

Keywords *- Lung And Colon Cancer, Histopathology Image Classification, Efficientnetb0, Cross-Attention Feature Fusion, Lc25000 Dataset.*

1. Introduction

Lung and colon cancers remain some of the most significant malignancies from a practical point of view, where early and accurate diagnosis is one of the most important factors in treatment. In conventional pathology analysis, Hematoxylin-Eosin (H&E) stained histopathological images are considered the gold standard for malignancy confirmation and tissue typing. However, manual microscopic analysis is a time-consuming, error-prone, and difficult process owing to the subtle transition in morphological patterns from benign tissue to adenocarcinoma patterns and squamous differentiation. This practical problem creates the need for computer-assisted diagnostic tools that can automatically learn significant features from digitized histopathological images, regardless of staining variations, complex tissue architecture, and the availability of annotated image samples. Deep learning has significantly pushed the state-of-the-art in histopathological image analysis, where CNNs can learn hierarchical representations of glandular patterns, nuclear texture, and spatial arrangements automatically without much engineering. But histopathological image classification is still faced with the following problems: (i) similar subtypes may share common color-texture statistics, (ii) variations in stains and scanners may result in variations in feature statistics, (iii) models may overfit dataset-specific patterns, and (iv) computationally intensive models may be hard to deploy in real-world applications. These problems are particularly relevant to multi-class lung-colon tissue classification, where successful discrimination must be shown to be achieved across different tissue classes with robust and repeatable learning pipelines.

1.1. Literature Review

The current state of research in the LC25000 lung-colon histopathology image classification problem is gradually shifting towards the transformer attention mechanism and efficient CNN backbones to improve class discriminability. Studies on transformer modeling have been demonstrated to improve global context aggregation, such as in Swin-Transformer models for lung and colon cancer histopathology

image classification, indicating that the windowed self-attention mechanism is more efficient in capturing long-range tissue patterns than local convolution operations [1]. At the same time, efficient CNN backbones and learning approaches have been investigated to efficiently balance accuracy and computational costs, such as Mobile/EfficientNet-based models and meta-heuristic optimization for improved convergence and generalization in LC25000 multi-class classification problems [2]. Learning pipelines tailored for lung and colon cancer histopathology image classification have also emphasized the importance of architectural modifications and training stability to address class confusion among visually similar classes [3].

The second approach relies on hybridization techniques that leverage deep features along with other informative features to improve robustness against stain and morphology variability. Feature fusion architectures that combine multiple families of features have been demonstrated to be effective in separating lung and colon cancers, for which the single-stream CNN feature alone is not sufficient [4]. The backbones of the EfficientNet family are generally preferred for their optimal accuracy/complexity trade-offs, including models that have been assessed for histopathology image classification accuracy and robustness for various types of cancers [5].

Other than the LC25000 challenge, multi-scale feature fusion architectures and lightweight CNN architectures have been investigated to jointly capture micro-texture and macro-structure patterns, which suggest that multiresolution information may have the potential to improve robustness for histopathology image classification [6].

In the context of colorectal histopathology image analysis, the application of attention mechanisms and transformer-aided models has been emerging for improved saliency learning and background tissue noise reduction. Coordinate attention and transformer models have been shown to improve the identification of colorectal cancer by focusing on diagnostically discriminative areas [7]. Feature fusion has also been improved by domain-specific transfer learning and multi-model fusion, proving that complementary learned features can be leveraged and combined for improved results in colorectal cancer histology. Explainability and interpretable learning are also active research areas, where lung cancer histopathology image analysis pipelines have integrated attention/saliency modules and post-hoc interpretability for improved trust and usability [8].

Recent studies also indicate a shift towards specialised models for difficult multi-cancer classification. Local-window vision transformers and attention-sparse models have been explored for multi-cancer histopathological image classification, indicating that well-designed attention can provide improved robustness with reduced computation. Further, detection-oriented models (region-based or object-based learning) have been used for colon cancer histopathology image analysis to accurately identify and classify cancerous regions better than global classifiers [9]. Other complementary studies continue to emphasize the need for stain-agnostic learning, balanced learning, and appropriate evaluation protocols for histopathology multi-class classification, including substantial evidence that robust generalization necessitates models capable of capturing both micro-texture and macro-tissue structure [10-12].

1.2. Problem Statement

Although considerable progress has been made, the LC25000 lung-colon histopathology image classification task is still challenging because of (i) inter-class similarity between benign and malignant regions, (ii) intra-class variability due to differences in glandular development, keratinization, necrosis, and stromal patterns, and (iii) the sensitivity of purely deep features to stain/illumination variations and dataset biases.

Furthermore, most of the current state-of-the-art attention models are computationally expensive, thus hampering their applicability in resource-limited environments. Thus, there is an urgent requirement for a technically sound and efficient approach that can enhance discrimination between the five classes of the LC25000 challenge by effectively exploiting complementary information while ensuring reproducibility and stable evaluation.

1.3. Dataset

The proposed work utilizes the LC25000 histopathology image dataset, which is divided into five folder-class categories corresponding to benign and malignant regions of lung and colon tissues. The dataset consists of 25,000 RGB images (5,000 images per class): benign colonic tissue, benign lung tissue, colon adenocarcinoma, lung adenocarcinoma, and lung squamous cell carcinoma.

The images are resized to 224×224 pixels and processed in a stratified split manner to maintain class proportionality between the training and testing splits. The multi-class nature and morphological similarities between the different types of lung cancers make LC25000 a relevant benchmark dataset for testing the effectiveness of robust feature learning and fusion approaches.

2. Materials and Methods

2.1. Data, Splits, and Preprocessing

The LC25000 histopathology dataset was used for lung/colon tissue classification. Images are organized into five categories: benign colon, benign lung, colon adenocarcinoma, lung adenocarcinoma, and lung squamous cell carcinoma.

All samples were read with OpenCV, converted from BGR to RGB, and resized to 224 × 224 to match the fixed input resolution of the convolutional encoder.

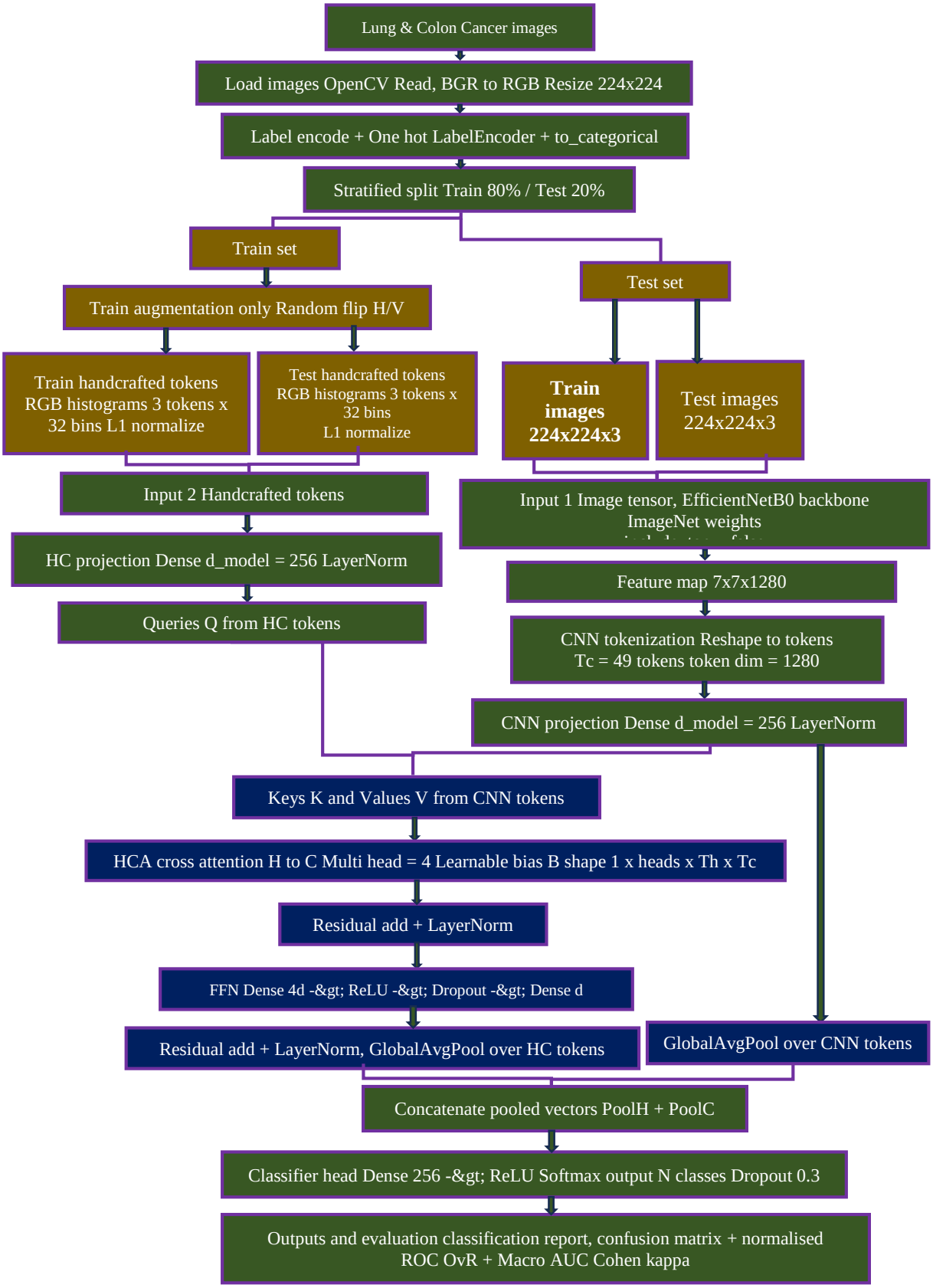

Fig. 1 Proposed HCA pipeline for five-class LC25000 histopathology classification

Class identifiers were taken from the directory names, encoded with a label encoder, and converted to one-hot vectors for the multi-class setting. We applied a stratified 80/20 train, test split to preserve class proportions across splits. Augmentation was performed only on the training set using random horizontal and vertical flips, improving orientation robustness while avoiding transformations that could alter diagnostically relevant stain–texture patterns.

2.2. Backbone Feature Extraction and Tokenization

For a given input RGB patch $x \in \mathbb{R}^{224\times224\times3}$, an EfficientNetB0 encoder (ImageNet initialisation, include_top=False) generates a dense convolutional feature map $F \in \mathbb{R}^{7\times7\times1280}$. This feature map is flattened over the spatial grid to extract a sequence of spatial tokens,

$$S \in \mathbb{R}^{T_c\times d_c}, T_c = 7\times7 = 49,\ d_c = 1280 \qquad (1)$$

With each token representing the local tissue morphology and subtle micro-texture patterns present within its receptive field. At the same time, we derive a complementary handcrafted representation directly from the RGB input by computing separate 32-bin histograms for each channel. This produces three histogram-based tokens (one per channel), which together give

$$H \in \mathbb{R}^{T_h\times d_h}, T_h = 3,\ d_h = 32 \qquad (2)$$

The resulting histograms are L1-normalized to enable fair comparison across patches and to reduce sensitivity to stain-intensity fluctuations. For attention-based fusion in a shared latent space, the learned spatial tokens and handcrafted tokens are each projected to a common model dimension $d = 256$ using trainable linear layers followed by Layer Normalization, yielding. $S' \in \mathbb{R}^{T_c\times d}$and $H' \in \mathbb{R}^{T_h\times d}$. We intentionally keep an asymmetric token budget, a few handcrafted tokens versus many spatial tokens, so the handcrafted branch remains lightweight while still guiding attention toward informative regions represented by the richer spatial stream.

2.3. Directional Projections for Cross-Attention

A directional fusion strategy is adopted in which handcrafted tokens act as queries, while CNN spatial tokens act as keys and values. Let $H' \in \mathbb{R}^{T_h\times d}$denote the projected handcrafted tokens and $S' \in \mathbb{R}^{T_c\times d}$denote the projected spatial tokens. Multi-head attention projections are defined as

$$Q = H'W_Q, K = S'W_K, V = S'W_V \qquad (3)$$

where $W_Q, W_K, W_V \in \mathbb{R}^{d\times d}$are learned matrices (implemented as bias-free dense layers). This assignment enforces an explicit inductive bias: stain/color statistics are treated as compact priors that query the spatial morphology tokens to emphasize diagnostically relevant regions before any global pooling.

2.4. Handcrafted-Guided, Bias-Aware Cross-Attention (Pre-Pooling Fusion)

The fusion module is based on a multi-head handcrafted-to-spatial cross-attention module with a learnable bias prior over token affinities. For head h, attention logits are computed as scaled dot products of handcrafted queries and spatial keys, biased by a trainable tensor Bthat captures stationary colour-region affinity patterns:

$$\text{Attn}(H', S') = \text{Softmax}\left(\frac{QK^{\top}}{\sqrt{d_h}} + B\right)V, \qquad (4)$$

Where $B \in \mathbb{R}^{1\times n_{heads}\times T_h\times T_c}$ is broadcast over the batch and initialized near zero. Unlike late fusion after pooling, Eq. (2) carries out token-level pre-pooling fusion, allowing the network to capture the delicate interactions between color and morphology, which are usually suppressed by early global averaging. The learnable bias prior helps to stabilize the attention weights by promoting consistent mapping between particular hand-crafted color statistics (queries) and spatial patterns (keys/values), without introducing a large number of parameters.

2.5. Post-Attention Integration and Classification Head

The output of cross-attention is incorporated into the handcrafted stream using residual learning to ensure the stability of the gradient and the retention of the original identity of the handcrafted token. This is achieved by adding the attention output back to H^\\prime after the application of Layer Normalization. A lightweight Feed-Forward Network (FFN) is then applied to refine the fused tokens through an expansion to 4d, followed by ReLU activation, dropout, and projection back to d, all wrapped around residual addition and Layer Normalization. Following the refinement of the fused tokens, two global pooling steps are applied: (i) global average pooling on the refined handcrafted tokens to obtain a compact representation of the fused prior vector, and (ii) global average pooling on the CNN spatial tokens to retain the global morphology information. The two vectors are then concatenated and fed into a small MLP head (Dense 256 + ReLU + Dropout 0.3) followed by a softmax output layer that predicts the probabilities of membership for the five LC25000 classes.

2.6. Training, Optimisation, and Reproducibility

The training of the models was carried out using the Adam optimizer with a learning rate of {10}^{-3}, categorical cross-entropy loss, and a mini-batch size of 32. Class weights were used to balance the classes. These weights were calculated based on the inverse frequency of the classes. Transfer learning was used, where the layers of the EfficientNetB0 model were frozen, with the exception of the last layers, which were unfrozen to enable adaptation to the task at hand. The augmentation process was limited to flipping during training. No test-time augmentation was carried out. All the preprocessing and encoding processes were

deterministic due to the fixed random seed used during the stratified split.

2.7. Evaluation Protocol

Performance was measured using accuracy, macro F1 score, macro AUC (one-vs-rest), and Cohen's kappa to account for both discrimination and agreement above chance for multi-class classification. Confusion matrices (unnormalized and row-normalized) were employed to analyze error patterns per class, and ROC curves were plotted per class for separability analysis. Figure 1 provides an overview of the entire pipeline: (i) LC25000 folder-wise data loading and resizing, (ii) parallel handcrafted token generation through RGB histograms, (iii) EfficientNetB0 spatial token extraction and projection, (iv) handcrafted-guided bias-aware cross-attention for pre-pooling fusion, (v) residual + FFN refinement, dual pooling, and (vi) final softmax classification.

2.8. Baselines, Ablations, and Intended Advantages

To situate the role of bias-aware pre-pooling fusion, the proposed HCA module is contrasted with attention and non-attention fusion baselines on the same split and training configuration: (i) a cross-attention variant that eliminates the bias prior B(handcrafted queries attend to CNN tokens without learned affinity bias), (ii) a stacked self-attention variant applied to the concatenated handcrafted and CNN token sequence (full sequence interaction without directional handcrafted guidance), and (iii) a simple concatenation + MLP fusion baseline that pools each stream and fuses only at vector level. These comparisons highlight the role of three design elements: fusion at the token level before pooling, directional query mapping (handcrafted \rightarrow\ spatial), and the learnable bias prior B that constrains color-region associations. The goal is to enable a lightweight yet powerful fusion layer that captures diagnostically informative colour-morphology interactions in a modular fashion that is compatible with standard convolutional encoders.

The proposed pipeline (Figure 1) standardizes image loading and preprocessing, and then builds dual-stream features: (i) deep feature tokens derived from an EfficientNetB0 backbone (ImageNet initialization, include_top=False) and tokenized from the final convolutional feature map, and (ii) handcrafted color distribution tokens calculated as channel-wise RGB histograms (3 tokens × 32 bins) with L1 normalization. The two token streams are projected into a shared embedding space and combined using a Handcrafted-Aware Cross-Attention mechanism, where handcrafted tokens serve as queries and CNN tokens as keys/values to focus attention on diagnostically informative deep regions. The combined representation is then refined with residual connections, layer normalization, and a feed-forward network, and pooled and concatenated for final softmax classification over the five classes of the LC25000 challenge.

The twist is in the token-level, directional fusion where the handcrafted RGB histogram descriptors are considered a compact stain-sensitive prior that explicitly guides the EfficientNetB0 patch-token attention, instead of just concatenating the pooled vectors. The handcrafted tokens are used as queries in the cross-attention mechanism, where the model learns a meaningful mapping between the global color distribution changes (commonly associated with stains and tissue composition) and the deep discriminative spatial patterns, while being computationally efficient because of the limited set of handcrafted tokens (T_h=3). This allows for complementary learning, where the handcrafted priors regularize the attention topography to be stable with respect to stain variations, and the deep tokens encode morphology, resulting in a fusion space that is more discriminative than single-stream CNNs or late concatenation for the LC25000 multi-class task.

3. Results and Discussion

All experiments were carried out on the five-class LC25000 setting with a stratified 80/20 split. The test split reported is balanced, with 150 images per class (750 in total), as evident from the per-class support in Tables 1-3. The following analysis begins with an examination of the three token fusion variants based on their class-wise performance (Tables 1-3), and then aggregates the results of comparison across all four methods (Table 4), with Figures 2-4 providing a graphical representation of the same. The Cross-Attention (no-bias) baseline (Table 1) performs at or very close to ceiling on all classes, with perfect precision/recall for benign lung tissue and very high scores for colon adenocarcinoma.

Table 1. Cross-Attn (no bias): class-wise performance on LC25000

Cross-Attn (no bias) Class	Precision	Recall	Specificity	F1	Support
benign colonic tissue	1	0.9933	1	0.9967	150
benign lung tissue	1	1	1	1	150
colon adenocarcinoma	0.9934	1	0.9983	0.9967	150
lung adenocarcinoma	0.9548	0.9867	0.9883	0.9705	150
lung squamous cell carcinoma	0.9862	0.9533	0.9967	0.9695	150

The remaining difficulty is focused on the clinically relevant lung types, where lung adenocarcinoma has a precision/recall/F1 of 0.9548/0.9867/0.9705, and lung squamous cell carcinoma has 0.9862/0.9533/0.9695. This trend suggests that even when directionally using handcrafted tokens to query deep spatial tokens, the removal of the bias prior to attention alignment leads to a greater reliance on sample-specific co-occurrences. Consequently, morphologically overlapping lung patterns are more likely than colon tissue patterns to introduce residual ambiguity under the same preprocessing and tokenization paradigm.

Table 2. Self-Attn (stacked): class-wise performance on LC25000

Self-Attn (stacked) Class	Precision	Recall	Specificity	F1	Support
benign colonic tissue	1	0.9733	1	0.9865	150
benign lung tissue	0.9934	1	0.9983	0.9967	150
colon adenocarcinoma	0.9677	1	0.9917	0.9836	150
lung adenocarcinoma	0.8938	0.9533	0.9717	0.9226	150
lung squamous cell carcinoma	0.971	0.8933	0.9933	0.9306	150

By contrast, the strongest degradation in overall discrimination is provided by the stacked Self-Attention baseline (Table 2), with the degradation again dominated by the lung categories. Specifically, lung adenocarcinoma falls to 0.8938 precision and 0.9226 F1, while lung squamous cell carcinoma falls to 0.8933 recall and 0.9306 F1.

While the full sequence self-attention mechanism allows for unconstrained interaction between handcrafted and CNN features, it also destroys the desired inductive bias of "handcrafted priors guiding spatial morphology." Without the directional bias, the network is free to spread attention over the concatenated token sequence, which seems to be sub-optimal for distinguishing the two lung malignancies with overlapping texture and staining distributions. The results for the benign classes and colon adenocarcinoma (Table 2 and Figure 2) indicate that the failure mode is not a general problem of feature insufficiency, but rather the lack of a stabilizing fusion bias for the hardest inter-lung boundary. The proposed HCA model (Table 3) improves the hard lung boundaries while keeping very high scores on the rest of the categories.

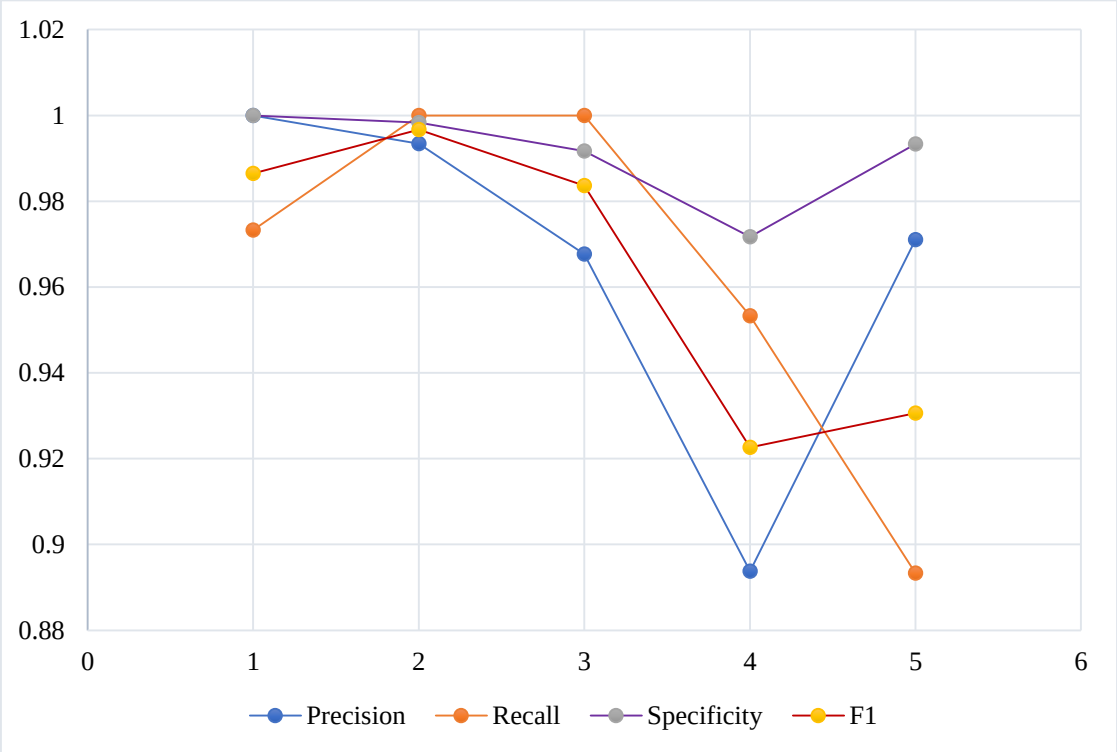

Fig. 2 Cross-Attn (no bias): result visualisation on LC25000

Table 3. Proposed HCA: class-wise performance on LC25000

Proposed HCA Class	Precision	Recall	Specificity	F1	Support
benign colonic tissue	1	0.98	1	0.9899	150
benign lung tissue	1	0.9867	1	0.9933	150
colon adenocarcinoma	0.9868	1	0.9967	0.9934	150
lung adenocarcinoma	0.9551	0.9933	0.9883	0.9739	150
lung squamous cell carcinoma	0.9932	0.9733	0.9983	0.9832	150

In comparison to the no-bias cross-attention baseline, the proposed approach improves the F1 measure for lung adenocarcinoma to 0.9739 and lung squamous cell carcinoma to 0.9832, while maintaining precision at or close to 1.0 for the benign components and near-perfect colon adenocarcinoma classification. The crucial takeaway here is that the learnable bias prior in HCA serves as a light-weight regulariser for the affinities of tokens, which helps to stabilize mappings from compact stain-sensitive histogram cues to recurring discriminative spatial patterns. This is most helpful exactly at the points where morphology and stain statistics overlap most between lung adenocarcinoma and lung squamous cell carcinoma, thus enhancing subtype discrimination without adding heavy architectural complexity. The aggregate-level comparison is verified by the integrated table in Table 4.

Table 4. Overall comparison of fusion strategies on LC25000

Model	Accuracy	Macro-F1	Macro AUC (OvR)	Cohen's kappa
Concat+MLP	0.9867	0.9867	0.9999	0.9833
Cross-Attn (no bias)	0.985	0.9842	0.9997	0.9831
Self-Attn (stacked)	0.964	0.964	0.9968	0.955
Proposed HCA (ours)	0.9947	0.9947	0.9999	0.9933

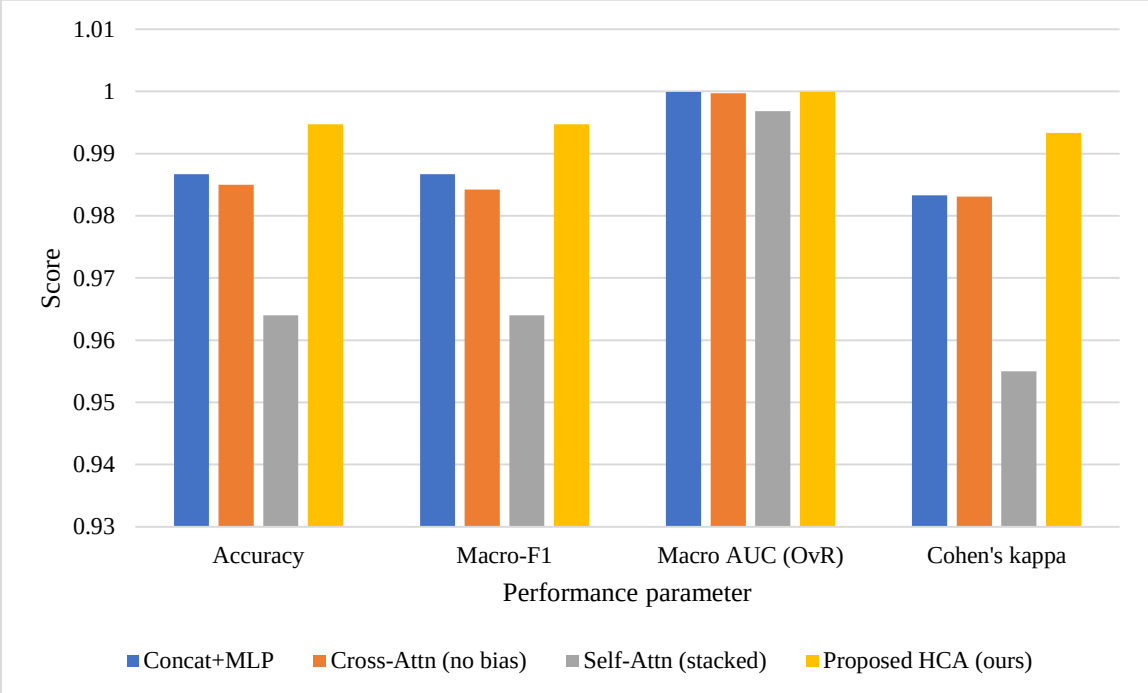

Fig. 3 Self-Attn (stacked): result visualization on LC25000

The proposed HCA model achieves the highest performance with 0.9947 accuracy, 0.9947 Macro-F1, and highest agreement $\kappa = 0.9933$, outperforming Concat+MLP (0.9867 accuracy, $\kappa = 0.9833$), Cross-Attention (no-bias) (0.985 accuracy, $\kappa = 0.9831$), and most notably the stacked Self-Attention baseline (0.964 accuracy, $\kappa = 0.955$). Although Macro-AUC scores are high for all models, the more informative trend is the simultaneous boost of Macro-F1 and

κ for the proposed model, which together indicate (i) robustness to class imbalance at the macro level and (ii) higher reliability above chance agreement for five-way classification, as illustrated in Figures 3 and 4. Together with the class-wise improvements in Table 3, the findings confirm that the design decisions critical to novelty, token-level pre-pooling fusion, directional handcrafted-to-spatial querying, and the learnable bias prior are indeed beneficial and lead to targeted improvements, especially for the most confusable categories of lung diseases in the LC25000 dataset.

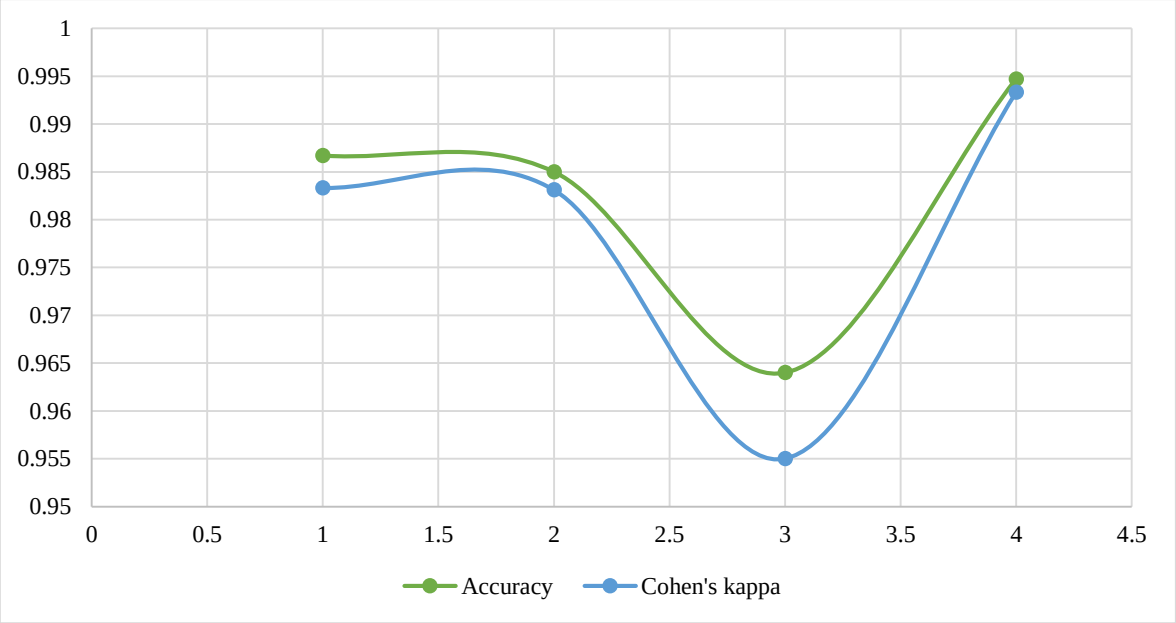

Fig. 4 Proposed HCA and Concat+MLP: result visualization on LC25000

4. Conclusion

In this study, we developed an EfficientNetB0-based hybrid model for five-class lung and colon histopathology classification using the LC25000 dataset. The central contribution is a handcrafted-aware cross-attention fusion module that integrates compact, stain-sensitive histogram tokens with deep spatial morphology tokens before pooling. By performing fusion at the token level, the network retains discriminative local cues that are often weakened or lost in conventional late-fusion designs.

We further introduce a learnable bias prior within the attention computation to stabilize handcrafted-to-spatial affinity learning. This is particularly beneficial when separating morphologically close lung subtypes, where subtle stain–texture differences influence class boundaries. Compared with (i) cross-attention without bias, (ii) stacked self-attention over concatenated tokens, and (iii) simple concatenation followed by MLP fusion, the proposed directional and bias-aware pre-pooling fusion provides stronger class-wise separability and improved overall agreement metrics. These results support the value of explicitly guiding CNN token features with lightweight handcrafted priors for multi-class histopathology recognition.

Future work will evaluate the framework on multi-institutional cohorts, investigate stain normalization and domain adaptation to improve generalisability, and explore slide-level aggregation strategies to extend the approach to whole-slide histopathology classification.

5. Data Availability Statement

The data used in this study are publicly available. Representative histopathology images for the five-class lung and colon tissue classification task were obtained from the LC25000 dataset, which is hosted in open research repositories. All preprocessing steps, experimental settings, and evaluation procedures required to reproduce the reported results are described in this manuscript. Model weights and implementation code will be shared by the authors upon reasonable request.

6. Author Contributions

Mullakuri Anusha: Conceptualisation, methodology, software implementation, data curation, experimentation, validation, formal analysis, visualisation, and drafting of the manuscript.

D. Srinivasulu Reddy: Supervision, investigation, resources, project administration, critical review and editing of the manuscript, and overall guidance.

7. Conflict of Interest

The authors declare no conflict of interest.

References

[1] Jie Ji et al., "Automated Lung and Colon Cancer Classification Using Histopathological Images," *Biomedical Engineering and Computational Biology*, vol. 15, pp. 1-8, 2024. [CrossRef] [Google Scholar] [Publisher Link]

[2] A. Hasib Uddin et al., "Colon and Lung Cancer Classification from Multi-Modal Images using Resilient and Efficient Neural Network Architectures," *Heliyon*, vol. 10, no. 9, pp. 1-23, 2024. [CrossRef] [Google Scholar] [Publisher Link]

[3] Raquel Ochoa-Ornelas et al., "A Robust Transfer Learning Approach with Histopathological Images for Lung and Colon Cancer Detection using EfficientNetB3," *Healthcare Analytics*, vol. 7, pp. 1-15, 2025. [CrossRef] [Google Scholar] [Publisher Link]

[4] MehmetGül, "An Effective Study on the Diagnosis of Colon Cancer with the Developed Local Binary Pattern Method," *Scientific Reports*, vol. 15, pp. 1-20, 2025. [CrossRef] [Google Scholar] [Publisher Link]

[5] Marwa Obayya et al., "Biomedical Image Analysis for Colon and Lung Cancer Detection using Tuna Swarm Algorithm with Deep Learning Model," *IEEE Access*, vol. 11, pp. 94705-94712, 2023. [CrossRef] [Google Scholar] [Publisher Link]

[6] Md. Al-Mamun Provath et al., "Classification of Lung and Colon Cancer Histopathological Images Using Global Context Attention Based Convolutional Neural Network," *IEEE Access*, vol. 11, pp. 110164-110183, 2023. [CrossRef] [Google Scholar] [Publisher Link]

[7] Indu Chhillar, and Ajmer Singh, "A Feature Engineering-Based Machine Learning Technique to Detect and Classify Lung and Colon Cancer from Histopathological Images," *Medical & Biological Engineering & Computing*, vol. 62, pp. 913-924, 2024. [CrossRef] [Google Scholar] [Publisher Link]

[8] Saeed Iqbal et al., "A Novel Heteromorphous Convolutional Neural Network for Automated Assessment of Tumors in Colon and Lung Histopathology Images," *Biomimetics*, vol. 8, no. 4, pp. 1-22, 2023. [CrossRef] [Google Scholar] [Publisher Link]

[9] Sunila Anjum et al., "Lung Cancer Classification in Histopathology Images Using Multiresolution Efficient Nets," *Computational Intelligence and Neuroscience*, vol. 2023, no. 1, pp. 1-12, 2023. [CrossRef] [Google Scholar] [Publisher Link]

[10] Omneya Attallah et al., "Lung and Colon Cancer Classification Using Multiscale Deep Features Integration of Compact Convolutional Neural Networks and Feature Selection," *Technologies*, vol. 13, no. 2, pp. pp. 1-28, 2025. [CrossRef] [Google Scholar] [Publisher Link]

[11] Mohammed Al-Jabbar et al., "Histopathological Analysis for Detecting Lung and Colon Cancer Malignancies Using Hybrid Systems with Fused Features," *Bioengineering*, vol. 10, no. 3, pp. 1-25, 2023. [CrossRef] [Google Scholar] [Publisher Link]

[12] Abdulkream A. Alsulami et al., "Identification of Anomalies in Lung and Colon Cancer Using Computer Vision-Based Swin Transformer with Ensemble Model on Histopathological Images," *Bioengineering*, vol. 11, no. 10, pp. 1-22, 2024. [CrossRef] [Google Scholar] [Publisher Link]